AIAA JOURNAL
Vol. 34, No. 3, March 1996

Validation of a Numerical Method for Extracting Liner Impedance

Willie R. Watson*
NASA Langley Research Center, Hampton, Virginia 23681-0001
Michael G. Jones†
Lockheed Engineering and Sciences Company, Inc., Hampton, Virginia 23666
and
Sharon E. Tanner‡ and Tony L. Parrott§
NASA Langley Research Center, Hampton, Virginia 23681-0001

We report the initial results of a test series to evaluate a method for extracting the normal-incidence impedance of a locally reacting, acoustically absorbing liner located on the lower wall of a duct in a grazing-incidence, multimodal, nonprogressive acoustic wave environment without flow. This initial evaluation tests the method's ability to converge to the known normal-incidence impedance of a solid steel plate, and to the normal-incidence impedance of an absorbing test specimen whose impedance has been measured in a conventional normal-incidence tube. The method converges to the normal-incident impedance values and thus is an adequate tool for extracting the impedance of specimens in a grazing-incidence, multimodal, nonprogressive acoustic wave environment for a broad range of source frequencies.

Nomenclature

$[A^{[I,J]}]$	= local element matrix
$[A(\zeta)]$, $[A_I]$, $[B_I]$	= complex block tridiagonal matrices
a, b	= length and height, respectively, of a finite element
c_0, ρ_0	= ambient sound speed and density, respectively
d	= cavity depth
$E(\varsigma, \eta)$	= field-equation error function
$EW(\varsigma)$	= wall error function
$\{F\}$	= vector containing source effects
f	= frequency, Hz
$f_1(\varsigma)$, $f_2(\varsigma)$	= one-dimensional basis functions
H, L	= height and length, respectively, of impedance-tube test section
I, J	= axial and transverse node numbers, respectively
IMAX, JMAX	= number of points in resistance and reactance grids, respectively
i	= $\sqrt{-1}$
k	= free-space wave number
L_1, L_2	= leading and trailing edges, respectively, of test specimen
M, N	= number of nodes in x and y directions, respectively
m	= number of upper-wall measurement points
N_1, N_2, N_3, N_4	= two-dimensional basis functions
$p(x, y)$	= complex acoustic pressure at (x, y)
p_1, p_2, p_3, p_4	= complex acoustic pressure at local nodes 1, 2, 3, and 4, respectively
p_{ref}	= reference pressure, 20 μPa
$p_s(y)$, p_{wall}	= acoustic source pressure and wall pressure, respectively
SPL	= measured sound pressure, dB (re 20 μPa)
t	= dimensional time
x, y	= Cartesian coordinates
$x_1, x_2, \ldots, x_m$	= locations of upper-wall microphones
β	= dimensionless admittance, $\xi + i\sigma$
ζ	= dimensionless wall impedance, $\theta + i\chi$
$\zeta_{\text{exit}}(y)$	= dimensionless exit impedance
η, ς	= local coordinate system for a finite element
$\{\Phi\}$	= global vector of complex acoustic pressures
$\{\Phi^{[I,J]}\}$	= local vector of complex acoustic pressures
ϕ	= measured phase angle for complex acoustic pressure
ω	= circular frequency

Received May 6, 1995; revision received Oct. 2, 1995; accepted for publication Oct. 6, 1995.

*Research Scientist, Aerodynamic and Acoustics Method Branch, Fluid Mechanics and Acoustics Division, M.S. 128.
†Principal Engineer, Research Division, 144 Research Drive.
‡Research Scientist, Structural Acoustics Branch, Fluid Mechanics and Acoustics Division, M.S. 463. Senior Member AIAA.
§Research Scientist, Structural Acoustics Branch, Fluid Mechanics and Acoustics Division, M.S. 463.

I. Introduction

HIGHLY efficient duct treatments for acoustic noise suppression continue to be a critical consideration in the achievement of environmentally acceptable commercial aircraft. To this end, a continuing concern in treatment technology is the accurate determination of the normal-incidence impedance of an acoustic material underneath the boundary layers of grazing flows. Methods for extracting the normal-incidence impedance in such environments typically fall into three categories: T-tube,[1] in-situ,[2,3] and propagation model, which is the subject of this paper. All three methods have advantages and disadvantages, depending on facilities available, instrumentation, and test liner construction or complexity. The disadvantages of the T-tube and in-situ methods are summarized by Armstrong et al.[4] However, these two methods serve as useful complements to the propagation-model method.

The propagation-model method is operationally convenient for extracting impedance spectra of test specimens in grazing-flow environments. Consequently, flow duct facilities have been designed to obtain the appropriate environment for duct propagation models. The current procedure is to use an infinite-waveguide propagation model to extract the impedance of the test specimen from the measured data (i.e., spatial attenuation and phase rate on the wall opposite the test liner) for a single, unidirectional propagating mode.[4-7] However, in real facilities, these idealized test conditions (i.e., unidirectional, single propagating mode) generally are

attained only approximately under the best laboratory conditions, and typically degrade severely with increasing mean flow. Additionally, many conventional test liner structures, and, in particular, the innovative liner structures currently under investigation, generate acoustic fields of greater complexity because of scattering of energy into higher-order modes. Although this may be a desirable result in achieving more efficient, broadband-absorbing structures, it is a complicating feature that cannot be handled by the traditional unidirectional, single-mode propagation-model method.

In a recent paper,[8] a method for extracting the acoustic impedance of a material installed as a finite-length wall segment of a duct carrying a nonprogressive multimodal sound field without flow was presented. The method was successful for an assumed infinite liner using analytically based input data, and the accuracy was not dependent upon whether installed test specimens were rigid or soft. The purpose of this paper is to validate the impedance extraction method using measured data and a finite-length liner. More specifically, the impedance extraction method developed in Ref. 8 is validated by testing the ability of the method to reproduce known normal-incidence impedance data for a solid steel plate and a sound-absorbing specimen. In contrast to the analytically based input data used in Ref. 8, all input data used in this report were obtained from acoustic pressure measurements taken in a grazing-incidence impedance-tube facility with the test specimen installed.

The remainder of this paper is organized into five sections. Section II describes the measurement system used to obtain the input data for the numerical method and gives a brief description of each test specimen. The governing equations and boundary conditions are presented in Sec. III. Section IV describes the numerical method that is used to extract the unknown impedance. The known normal-incidence impedances for the specimen are used as baselines against which the accuracy of the model is judged; these results are presented in Sec. V. Finally, conclusions relevant to this paper and ongoing research activities are presented in Sec. VI.

II. Experimental Setup and Test Specimens

The input data used to extract the impedance of each test specimen were obtained from measurements using a flow-impedance tube in the NASA Langley Flow Impedance Laboratory. This multiconfigurational apparatus has a 51 × 51 mm cross section and is designed to produce a controlled aeroacoustic environment with a Mach number up to 0.6 over a test specimen length of 41 cm. Four 120-W phase-matched acoustic drivers generate signals over a frequency range of 0.3–3.0 kHz, with sound pressure levels up to 155 dB at the test specimen leading edge. In the present investigation, there was no mean flow. Sound pressure levels of at least 120 dB at each frequency of interest were set at the leading edge of the test specimen. A schematic of the flow-impedance tube is provided in Fig. 1. The test section (section of the duct between the source and the exit plane) is 84 cm long. The upper and two side walls of the test section are stainless steel.

Acoustic waves are propagated from left to right, across the surface of the test specimen, and into a termination section designed to minimize reflections over the frequency range of interest. Two 6-mm condenser-type microphones were flush-mounted in the test section, one at a fixed location on the side wall, and the other on an axial traverse bar. A 13-mm-wide precision-machined slot in the top wall of the flow-impedance tube allows this axial traverse bar to traverse the test section length by means of a computer-controlled digital stepping motor. The fixed-location microphone was used to provide a reference for amplitude and phase measurements. The data acquisition program automatically positioned the traversing microphone at several preselected locations, ranging from 18 cm upstream of the leading edge to 52 mm downstream of the trailing edge of the test specimen. At each measurement location a transfer function between the traversing and the fixed microphones was measured and used to determine the sound pressure level and phase relative to the fixed microphone. The complex acoustic pressure at the wall location is determined from the equation

$$p_{\text{wall}} = p_{\text{ref}} 10^{20/SPL} e^{i\phi} = p_{\text{ref}} 10^{20/SPL} (\cos\phi + i \sin\phi) \qquad (1)$$

A block diagram of the electronic instrumentation and signal conditioning system is given in Fig. 2. At each test frequency, a sound pressure level was set at the test specimen leading edge with a signal generator.

The duct propagation model, which is discussed in the following section, requires a measurement of three sets of input data: 1) the upper-wall acoustic pressure, 2) the source-plane acoustic pressure, and 3) the exit-plane impedance.

Unfortunately, the source-plane acoustic pressure and exit-plane impedance are functions of position in these planes. Therefore, transverse-probe microphones are needed to obtain these data when the test specimen is installed. However, a transverse-probe microphone was not available for this initial investigation. The experiment therefore was designed carefully to minimize higher-order mode effects in the source and exit planes. All data for the duct propagation model were obtained from measurements made by the upper-wall traversing microphone. Because of the sound-absorbing properties of the liner, it is not possible to avoid high-order mode effects in the liner region. In addition, high-order mode effects and reflections will occur near the leading and trailing edges of the specimen.

To avoid the need of a transverse probe, the source plane was chosen 18 cm upstream (3.5 duct diameters) of the leading edge of the test specimen in the hardwall section of the duct, and the source frequency was kept below the cut on of higher-order hardwall modes. Higher-order mode effects caused by the presence of the test specimen are expected to decay upstream of the leading edge of the test specimen. Therefore, the source pressure at each point in the source plane was set to the value measured at the upper-wall microphone location. A similar procedure was applied at the exit plane. The exit plane was located 25 cm downstream (5 duct diameters) of the trailing edge of the test specimen, also in the hardwall section of the duct. The method described in Ref. 9 was used, with a hardwall test specimen installed to obtain the exit impedance. This was done by measuring complex acoustic pressures at five locations along the top wall of the impedance tube using the axial-traverse bar-mounted microphone. The same exit impedance was used for both the hardwall and the conventional liner configurations. Because the exit plane is 5 duct diameters downstream of the trailing edge of the liner and higher-order modes are cut-off, higher-order modes generated by the installation of the liner are not expected to carry appreciable acoustic energy to the exit plane. Thus, the exit impedance values at all points in the exit plane were set to that obtained at the upper wall.

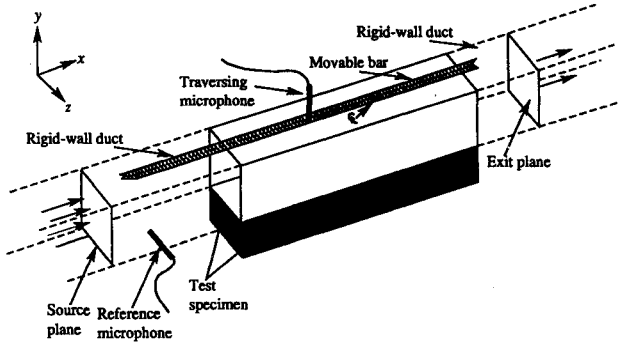

Fig. 1 Schematic of the Langley flow-impedance tube.

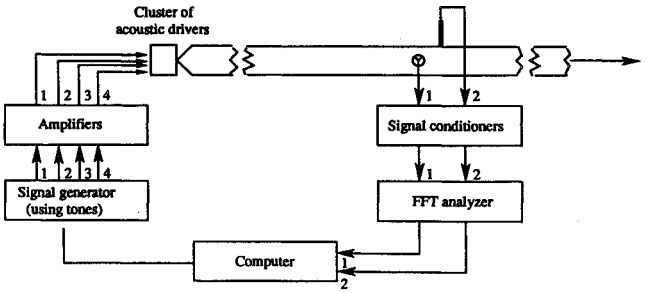

Fig. 2 Electronic instrumentation and signal conditioning system for the flow-impedance tube.

Input data were obtained for two specimens. The first specimen was a stainless steel plate (hardwall test specimen) for which the impedance was known. The second (a sound-absorbing specimen) was a conventional uniform liner that consisted of a fibermetal face sheet with a flow resistance of 100 k/m^2·s bounded to a 100-mm-deep aluminum hexcell honeycomb structure backed by a rigid plate. This type of liner structure has been used by the aeronautics industry for at least 35 years. Installed, this test specimen spanned the 51-mm width of the test section for a length of 41 cm. Normal-incidence impedance measurements for this sound-absorbing specimen were obtained using a conventional normal-incidence impedance tube measurement, identical to that of Jones and Parrott.[9] Because of the simplification that the absence of mean flow affords, the measured normal-incidence impedances and the impedances extracted using the method described in this report (grazing-incident sound) are expected to compare favorably. Thus, the measured normal-incidence impedance is used as a baseline against which to judge the accuracy of the impedance extraction method when flow is absent.

III. Governing Equation and Boundary Conditions

A brief description of the governing equation and boundary conditions used to extract the impedance of each test specimen is presented. Figure 3 depicts the applicable geometry and coordinate system used to model the test section of the Langley flow impedance tube. The axial and transverse (vertical) directions are denoted by x and y, respectively. The spanwise direction, normal to the (x, y) plane, is not shown in the figure. To limit the propagation model to two dimensions, plane waves are assumed in the spanwise direction. This is a reasonable assumption since the side walls of the impedance tube are rigid and the sound frequency is below the cut on of any higher-order modes in the hardwall section. The lower and upper walls of the duct are located at $y = 0$ and H, respectively, and are also rigid except where the liner is. The source and exit planes are located in the hardwall section of the duct at $x = 0$ and L, respectively. The test specimen (assumed locally reacting) is installed in the lower wall and has a normalized impedance $\zeta = \theta + i\chi$. The leading and trailing edges of the specimen are at $x = L_1$ and L_2, respectively. To perform the computation for the hardwall specimen (i.e., the stainless steel plate), it is convenient to use the acoustic admittance of the specimen, defined as $\beta = \xi + i\sigma$. Measurement points are located along the upper wall at $x = x_1, x_2, x_3, \ldots, x_m$ as shown. Acoustic pressure measurements at these locations were obtained with the traversing microphone as described in the preceding section.

The mathematical problem is to find the solution to the Helmholtz equation

$$\frac{\partial^2 p(x, y)}{\partial x^2} + \frac{\partial^2 p(x, y)}{\partial y^2} + k^2 p(x, y) = 0 \tag{2}$$

A time convention of the form $e^{i\omega t}$ is used throughout this paper. In the source plane of the duct ($x = 0$), the sound pressure level and phase of the acoustic pressure field are measured and expressed as a complex pressure, $p_s(y)$, using Eq. (1). The source-plane boundary condition is therefore

$$p(0, y) = p_s(y) \tag{3}$$

The boundary conditions along the rigid upper wall and the rigid portion of the lower wall are equivalent to the requirement that the gradient of the acoustic pressure normal to the wall vanishes:

$$\frac{\partial p}{\partial y} = 0 \tag{4}$$

At the exit plane ($x = L$), the ratio of acoustic pressure to axial velocity is assumed to equal the exit impedance

$$\frac{\partial p(L, y)}{\partial x} = \frac{-ikp(L, y)}{\zeta_{\text{exit}}(y)} \tag{5}$$

Throughout this work, all impedances are normalized with respect to the characteristic impedance $\rho_0 c_0$ of the air in the duct. The test specimen is assumed to be locally reacting. Therefore, the boundary condition along the lower-wall portion of the duct containing the test specimen is

$$\frac{\partial p}{\partial y} = \frac{ikp}{\zeta(x)} \tag{6}$$

Equations (2–6) constitute a boundary value problem that can be solved to determine the unknown impedance, $\zeta(x)$, provided the upper-wall pressure is known.[8] The solution for the unknown impedance can be put in terms of known functions only for special cases of the boundary conditions and upper-wall pressure. These cases are not useful for general application. Therefore, the unknown impedance $\zeta(x)$ must be extracted by a numerical method for cases of practical interest.

IV. Numerical Method

The numerical method chosen to extract the unknown impedance of the lower wall is discussed in Ref. 8, and only sufficient detail is presented here for continuity and completeness. Because the experimental setup was designed to minimize higher-order mode effects, this discussion will assume a constant source pressure p_s, exit impedance ζ_{exit}, and lower-wall impedance ζ. However, in the most general application of the method, these functions need not be constants to successfully apply the method.[8] When applied to the current acoustic problem, the method may be interpreted as an approximation of the continuous acoustic field as an assemblage of rectangular finite elements, as illustrated in Fig. 4. It is assumed that there are N nodes in the axial and M nodes in the transverse directions of the duct. A typical rectangular element $[I, J]$ is shown in Fig. 5. Each element consists of four local node numbers labeled 1, 2, 3, and 4, respectively. Each element is considered to have width $a = (x_{I+1} - x_I)$ and height $b = (y_{J+1} - y_J)$ as shown. The objective of the method is to determine the impedance ζ that minimizes the difference between the upper-wall pressure obtained from the finite element solution and that obtained from measured data with the specimen installed.

To begin, Galerkin's finite element method is employed to minimize the field error. The field error is distinct from the wall error function, which will be used to extract the unknown impedance. First, define the local coordinates, ς and η, for the element

$$\varsigma = x/a \qquad \eta = y/b \tag{7}$$

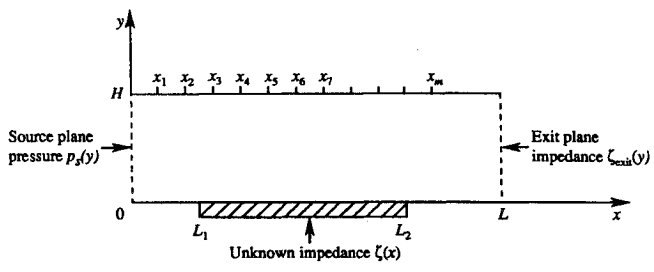

Fig. 3 Modeled portion of the Langley flow-impedance tube and coordinate system.

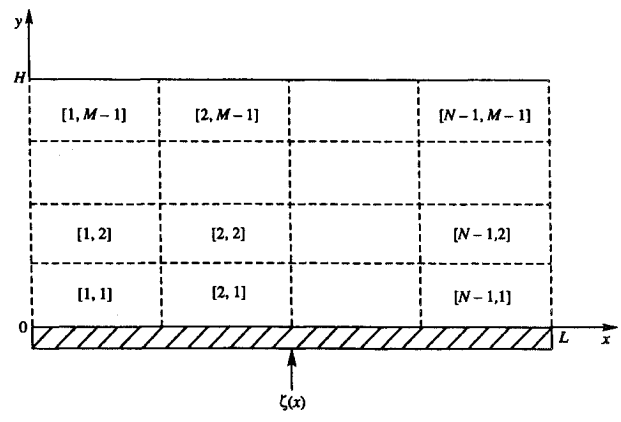

Fig. 4 Finite element discretization of the two-dimensional duct.

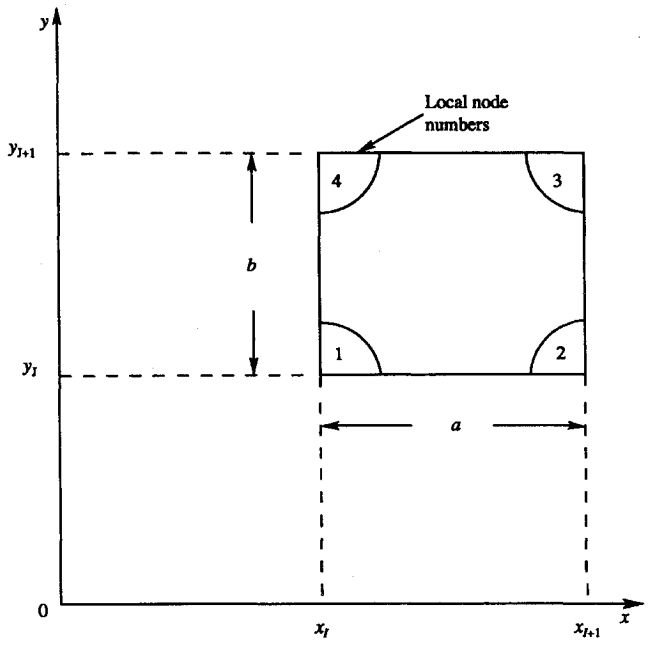

Fig. 5 Typical finite element and local-node numbering system.

Now, define the field error function as

$$E(\varsigma, \eta) = \frac{\partial^2 p(\varsigma, \eta)}{\partial \varsigma^2} + \frac{\partial^2 p(\varsigma, \eta)}{\partial \eta^2} + k^2 p(\varsigma, \eta) \tag{8}$$

Within each element, $p(\varsigma, \eta)$ is represented as linear combination of four functions, N_1, N_2, N_3, and N_4, which comprise a complete set of basis functions

$$p(\varsigma, \eta) = N_1(\varsigma, \eta)p_1 + N_2(\varsigma, \eta)p_2 + N_3(\varsigma, \eta)p_3 + N_4(\varsigma, \eta)p_4 \tag{9}$$

$$N_1(\varsigma, \eta) = f_1(\varsigma)f_1(\eta) \tag{10}$$

$$N_2(\varsigma, \eta) = f_2(\varsigma)f_1(\eta) \tag{11}$$

$$N_3(\varsigma, \eta) = f_2(\varsigma)f_2(\eta) \tag{12}$$

$$N_4(\varsigma, \eta) = f_1(\varsigma)f_2(\eta) \tag{13}$$

$$f_1(\varsigma) = 1 - \varsigma \tag{14}$$

$$f_2(\varsigma) = \varsigma \tag{15}$$

In an ideal sense, the solution to the sound field is obtained when the field error $E(\varsigma, \eta)$ is zero at each point of the computational domain. This is approximately achieved by requiring that the field error function be orthogonal to each basis function $N_I(\varsigma, \eta)$. Contributions to the minimization of the field-error function from a typical element are

$$ab \int_0^1 \int_0^1 E(\varsigma, \eta) N_I(\varsigma, \eta)\, d\varsigma\, d\eta = \left[A^{[I,J]}\right]\left\{\Phi^{[I,J]}\right\} \tag{16}$$

where $[A^{[I,J]}]$ is a 4×4 complex matrix for each element $[I, J]$, and $\{\Phi^{[I,J]}\}$ is a 4×1 column vector containing the unknown acoustic pressure at each of the four nodes of the element. The coefficients in the local matrix $[A^{[I,J]}]$ were computed in closed form. Note that the second-derivative terms in the field-error function $E(\varsigma, \eta)$ were integrated by parts so that linear-basis functions could be used. Also, the wall and exit-plane boundary conditions were substituted into these integrated terms.

Assembly of the global equations for the computational domain is a basic procedure in the finite element method. Appropriate shifting of rows and columns is all that is required to add the local element matrix $[A^{[I,J]}]$ directly into the global matrix $[A]$. Assembling the

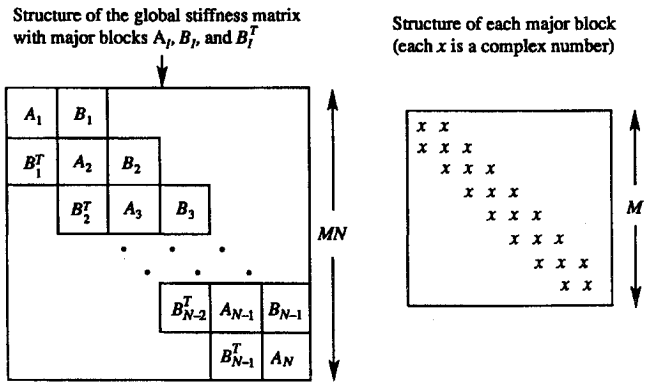

Fig. 6 Structure of the global matrix and major blocks.

elements for the entire domain results in a matrix equation of the form

$$[A(\zeta)]\{\Phi\} = \{F\} \tag{17}$$

where $[A(\zeta)]$ is a complex matrix whose order is MN, and $\{\Phi\}$ and $\{F\}$ are $MN \times 1$ column vectors. The vector $\{\Phi\}$ contains the nodal values of the unknown acoustic pressure and $\{F\}$ is the zero vector until the pressure source condition is imposed. It is necessary to apply the source condition to Eq. (17) before a solution can be obtained. Satisfying the noise-source boundary condition consists simply of setting all nodal values of acoustic source pressure in the source plane to the known value of source pressure; this introduces nonzero elements into the first M components of $\{F\}$.

The global matrix $[A(\zeta)]$ generated by Galerkin's method following application of the source condition is a complex symmetric matrix. Fortunately, owing to the discretization scheme used, it also will be block tridiagonal. The structure of the matrix $[A(\zeta)]$ after imposing source conditions is shown in Fig. 6, where the superscript T denotes matrix transposition. Note that $[A(\zeta)]$ is a square block tridiagonal matrix whose order is MN. This global matrix contains a number of major blocks (A_I, B_I), which are themselves square and block tridiagonal, as shown in the figure. The matrix elements in each major block are computed explicitly in terms of the yet unspecified impedance ζ. Much practical importance arises from this bock tridiagonal structure because it is convenient for minimizing storage and maximizing computational efficiency. Special matrix techniques exist for a solution of this structure. (Gaussian elimination with partial pivoting and equivalent-row infinity norm scaling is used to reduce the rectangular system to upper triangular form. Back substitution is then used to obtain the solution for the acoustic pressure at the MN node points.) All computation and storage are performed only on the elements within the bandwidth of the matrix $[A(\zeta)]$. The unknown impedance ζ of the acoustic material is determined from the measured upper-wall acoustic pressure. The procedure is to determine the impedance ζ such that the pressure along the top wall reaches its measured value at each of the measurement points x_I. The procedure consists of repeatedly cycling through the solution to Eq. (17), obtaining a set of upper-wall pressures for each impedance value. As each new set of wall pressures is computed, it is compared to the measured value until convergence is achieved.

The idea is best illustrated as follows for a lumped resistance in combination with a backing cavity. Define the unknown impedance as

$$\zeta = \theta + i\chi \tag{18}$$

where θ is the resistance and χ the reactance. Resistance values are positive, whereas reactance values span the real axis

$$0 \le \theta \le \infty, \qquad -\infty \le \chi \le \infty \tag{19}$$

It should be apparent that searching the entire upper half plane of the resistance/reactance space for the unknown impedance is impractical. Therefore, introduce the transformation

$$\chi = \cot(kd), \qquad 0 \le kd \le \pi \tag{20}$$

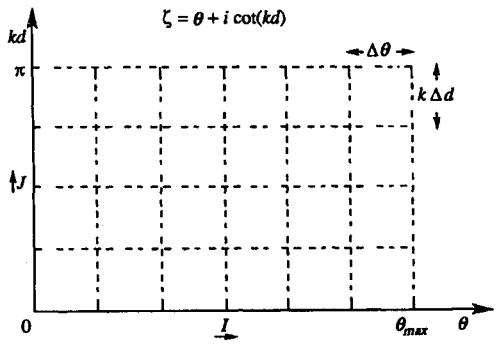

Fig. 7 Impedance grid in the complex plane.

and search for the unknown impedance in the (θ, kd) plane, where θ is limited to $0 \leq \theta \leq 10$, from practical considerations.

The complex plane (θ, kd) is now divided into *IMAX* evenly spaced intervals in the θ direction and *JMAX* evenly spaced points in the kd direction, as shown in Fig. 7. The increment spacing $\Delta\theta$ and $k\Delta d$ are

$$\Delta\theta = \frac{10}{IMAX - 1}, \qquad k\Delta d = \frac{\pi}{JMAX - 1} \tag{21}$$

Thus, a point $\zeta = \zeta_{IJ}$ in this uniform impedance grid is

$$\zeta_{IJ} = \theta_I + i\chi_J, \qquad \theta_I = (I-1)\Delta\theta, \qquad \chi_J = \cot(J-1)k\Delta d \tag{22}$$

If the measured upper-wall pressures with the specimen installed are $p_{\text{wall}}(x_n, H)$, and those computed from the finite element solution with ζ replaced by ζ_{IJ} are $p(x_n, H)$, then a measure of the closeness of ζ_{IJ} to ζ is given by the normalized wall-error function $EW(\zeta_{IJ})$

$$EW(\zeta_{IJ}) = \frac{\overline{EW}(\zeta_{IJ})}{\bar{E}_{\max}} \tag{23}$$

$$\overline{EW}(\zeta_{IJ}) = \frac{1}{m}\sum_{n=1}^{m} |p_{\text{wall}}(x_n, H) - p(x_n, H)| \tag{24}$$

in which $|\ |$ denotes the absolute value of a complex quantity, $\bar{E}_{\max}$ is the maximum value of $\overline{EW}$ for all points ζ_{IJ} in the impedance grid, and m is the number of known wall pressures.

Extraction of the unknown impedance of the material is now recast as a minimization problem. Thus, ζ should be chosen such that $EW(\zeta)$ is a global minimum. The global minimum is obtained using a two-step method. First, use a coarse grid in the impedance plane and tabulate the normalized wall-error function to determine the location (θ, kd) in that grid that produces an approximate minimum (θ^1, kd^1). Next, use a fine grid centered on (θ^1, kd^1) to obtain a new minimum. The location of the minimum of this fine grid corresponds to the unknown impedance ζ of the material. Coarse-grid calculations are performed with $IMAX = 51$, $JMAX = 31$, and $\Delta\theta = k\Delta d = 0.1$. Fine-grid calculations are carried out using $IMAX = JMAX = 21$, and $\Delta\theta = k\Delta d = 0.01$. The coarse-and fine-grid discretizations were determined from numerical experimentation in an earlier work.[8]

V. Results

A computer code carrying out the impedance extraction method has been developed. The finite element matrix equation (17) is solved using a highly developed software package, and minimization of the normalized wall-error function is performed internally by an in-house computer code. The unknown impedance ζ is returned by the in-house code. Results were computed using a workstation and were not computationally intensive (i.e., requiring only 0.5 s of CPU time for each point in the impedance grid). Analysis of the solid steel plate, for which the known admittance is nearly zero $(\beta = \xi + \sigma i \cong 0 + 0i)$, was conducted in the admittance plane for the sake of convenience. A 231 × 21 evenly spaced grid was used ($N = 231$ and $M = 21$) in the finite element discretization for all calculations. This grid ensured that a minimum of ten elements per axial wavelength was used in the finite element discretization at the highest frequency of interest.

Table 1 Exit impedances and wall conductances for the steel plate

Frequency, f, Hz	Measured exit impedance		Conductance of hardwall test specimen		
	θ	χ	Known	Extracted	Error
500	1.03	0.02	0.00	0.01	0.01
600	0.97	0.03	0.00	0.01	0.01
700	1.05	−0.01	0.00	0.01	0.01
800	1.05	−0.01	0.00	0.00	0.00
900	1.03	−0.06	0.00	0.00	0.00
1000	0.98	−0.04	0.00	0.00	0.00
1100	0.98	−0.03	0.00	0.00	0.00
1200	0.94	0.02	0.00	0.00	0.00
1300	0.97	0.07	0.00	0.00	0.00
1400	1.01	0.05	0.00	0.00	0.00
1500	1.02	0.06	0.00	0.00	0.00
1600	1.11	0.01	0.00	0.01	0.01
1700	1.05	−0.05	0.00	0.01	0.01
1800	1.04	−0.06	0.00	0.00	0.00
1900	0.95	−0.10	0.00	0.01	0.01
2000	0.92	−0.05	0.00	0.00	0.00
2100	0.91	0.02	0.00	0.00	0.00
2200	0.92	0.06	0.00	0.00	0.00
2300	0.99	0.12	0.00	0.00	0.00
2400	1.07	0.07	0.00	0.00	0.00
2500	1.10	0.08	0.00	0.01	0.01
2600	1.13	−0.07	0.00	0.01	0.01
2700	1.05	−0.11	0.00	0.01	0.01
2800	0.99	−0.12	0.00	0.02	0.02
2900	0.90	−0.10	0.00	0.01	0.01
3000	0.87	0.00	0.00	0.01	0.01

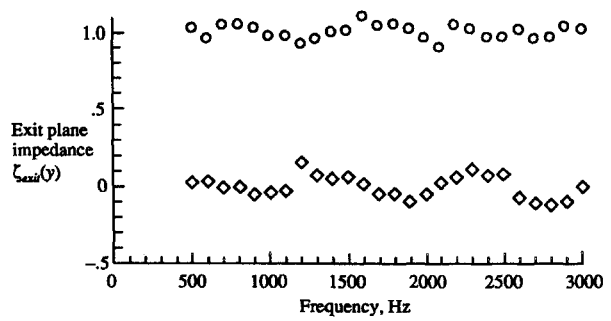

Fig. 8 Measured exit impedance for the Langley flow-impedance tube: ○, resistance and ◇, reactance.

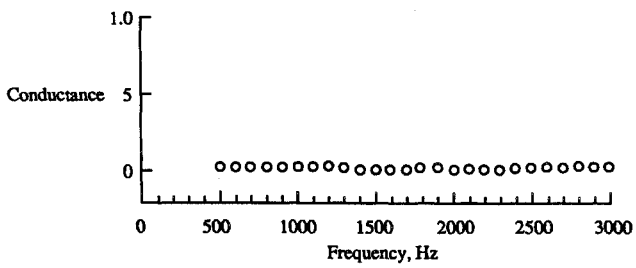

Fig. 9 Extracted conductance for the hardwall test specimen.

Figure 8 shows a plot of the measured resistance and reactance of the normalized exit impedance as a function of frequency. Note that reflections are present in the test section since the resistance is not unity and the reactance has a nonzero value. Thus, the acoustic field in the Langley flow-impedance tube is not purely progressive, even for the hardwall test specimen. The measured resistance and reactance spectra of the exit impedance are tabulated in the second and third columns respectively, of Table 1. Resistance values range from a minimum of 0.87 at 3000 Hz to a maximum of 1.13 at 2600 Hz. Reactance values range from a minimum of −0.12 at 2800 Hz to a maximum of 0.12 at 2300 Hz.

Hardwall admittances extracted using the method proposed in this study are shown first. The extracted normalized conductances ξ for the hardwall test specimen are shown in Fig. 9. Results are

Table 2 Extracted and measured impedance for the conventional liner

Frequency,	Resistance			Reactance		
f, Hz	Extracted	Measured	Error	Extracted	Measured	Error
500	0.39	0.44	−0.05	−0.55	−0.66	0.11
1100	0.46	0.40	0.06	−0.68	−0.61	−0.08
1500	0.53	0.63	−0.10	2.28	2.48	−0.20
2000	0.72	0.73	−0.01	−1.37	−1.47	0.10
2500	0.53	0.45	0.08	0.09	0.17	−0.08
3000	0.42	0.49	−0.07	1.35	1.30	0.05

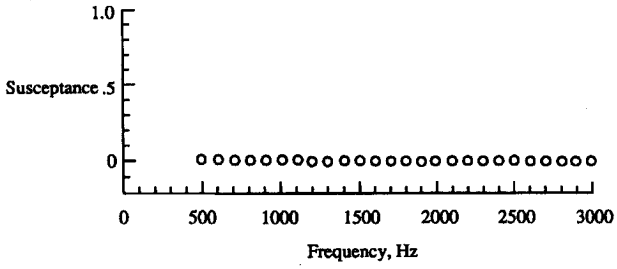

Fig. 10 Extracted susceptance for the hardwall test specimen.

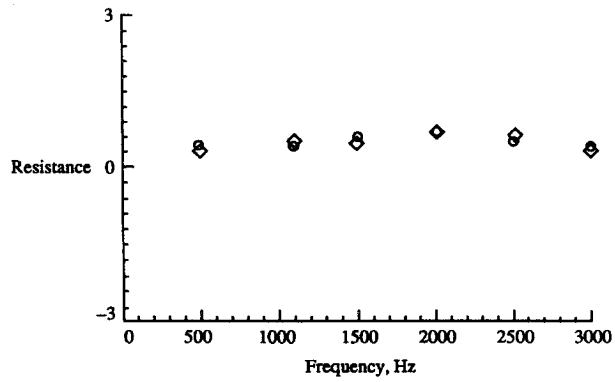

Fig. 11 Measured and extracted resistances for the conventional liner: ◇, measured and ○, predicted.

shown for 26 frequencies ranging from 500 to 3000 Hz in 100-Hz increments. The known and extracted conductance values are tabulated in the fourth and fifth column, respectively, of Table 1. The sixth column of Table 1 is the error (difference between known and extracted conductance values). The maximum error in the extracted conductance is only 0.02 (see tabulated results at 2800 Hz). Figure 10 shows a graph of the extracted susceptance σ. The extracted and known susceptances, truncated to two decimal digits of accuracy, were zero at each frequency; therefore, tabular results are not shown. The conductance and susceptance extracted using the measured input data appear as accurate as those extracted in Ref. 8 (i.e., impedance extractions were accurate to two decimal digits of accuracy) for analytically based input data, with a solid surface installed.

An appropriate next step in the validation of the impedance extraction method is to compare extracted and measured values for the conventional liner. The liner and end effects allow generation of higher-order modes and reflections in the test section that were not present for the solid steel plate. Figure 11 shows a comparison of the extracted and measured resistances, θ, for the conventional liner at six selected frequencies (500, 1100, 1500, 2000, 2500, and 3000 Hz). Extracted and measured resistance values for the conventional liner are tabulated in the second and third columns, respectively, of Table 2. Extracted resistance values range from a minimum of 0.39 at 500 Hz to a maximum of 0.72 at 2000 Hz. At each frequency, the extracted values are close to the measured values. A maximum error of −0.01 is observed in the extracted resistance at 1500 Hz (see fourth column of Table 2). Figure 12 shows a comparison of extracted and measured reactances for the conventional liner. The data for this graph are tabulated in the fifth and sixth

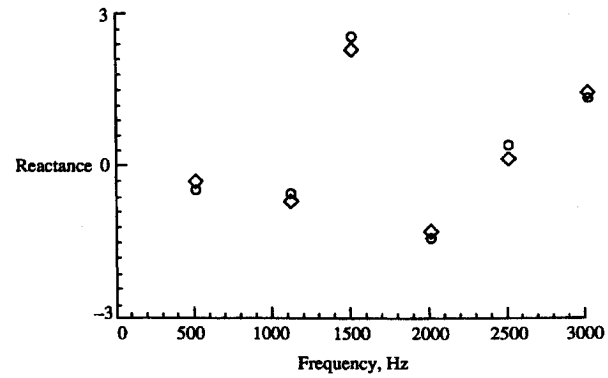

Fig. 12 Measured and extracted reactances for the conventional liner: ○, measured and ◇, predicted.

columns, respectively, of Table 2. The variability in the reactance component of the impedance is noticeably greater than that of the resistance component. The maximum error in the extracted reactance is −0.20 and occurs at 1500 Hz (see column seven of Table 2). Note that extracted reactance values are generally less accurate than the extracted resistance values.

Since the largest error in the extracted and measured normal-incidence impedances for the soft specimen occurred at 1500 Hz, each impedance value was used to predict the attenuation of the soft test specimen with the prediction program. The attenuation predicted with the measured normal-incidence impedance ($\zeta = 0.63 + 2.48i$) was 1.70 dB, and that obtained using the extracted impedance ($\zeta = 0.53+2.28i$) was 1.67 dB. Thus, for the chosen soft test specimen, the difference between the extracted and measured normal-incidence impedances (i.e., 0.1 for resistance and −0.2 for reactance) does not affect the total noise reduction performance of the test specimen.

Extracted resistance and reactance with the liner installed match the measured normal incidence values quite well. However, the extracted values are not as good as those extracted for the hardwall specimen. This is in contrast to the extracted impedances obtained in Ref. 8 with analytically based data, in which the extracted impedances were just as accurate for soft as for rigid walls (i.e., two decimal digits of accuracy for hard and soft specimens). There are several possible explanations as to why the extracted impedances are less accurate with the liner installed when experimentally based input data are used. These are as follows:

1) Twenty elements across the duct may not be sufficient to resolve the transverse acoustic field in the neighborhood of the discontinuities at the leading and trailing edges of the test specimen.

2) Installation of the liner generates some transverse dependence in the acoustic field at either the source or exit plane (these effects have been neglected in the impedance extractions).

3) Differences between the extracted and measured values may be because of small errors in the measured normal-incident impedance determination.

A more likely explanation is that a combination of these effects is responsible for a less accurate impedance extraction when the liner is installed.

VI. Conclusions and Discussion

A numerical method for extracting the acoustic impedance of a test specimen under grazing-incidence sound using measured data has been tested for its effectiveness. Although the method as presented here does not contain flow effects, it is extendable to mean flows with shear. Results of this study show that the method is effective in extracting the impedance of hard or soft specimens for a range of source frequencies. There is only a slight degradation in the accuracy of the extracted impedance when high-quality measured data are used instead of analytically based data.

The results of this investigation represent a significant step in the development of a new impedance extraction technique. This method currently extends zero-flow impedance prediction capability to test specimens with nonuniform impedance distributions in nonprogressive acoustic wave fields, while maintaining impedance accuracy.

Additional validation experiments are planned, which should 1) validate the measurement capability for more complicated sources and at higher frequencies, 2) validate the applicability of the method to variable impedance liners, and 3) validate the method for a range of liner thicknesses (i.e., impedances).

Efforts are also under way to include the effects of shearing flows in the impedance extraction technique. One important challenge in both the flow and the zero-flow efforts is to provide sufficiently accurate boundary condition data at the source and exit planes such as prescribed by Eqs. (3) and (5). Recall that, in the source plane, the complex acoustic pressure distribution is required (also, the entrance impedance when flow is present), whereas in the exit plane the exit impedance distribution is required.

Presumably, the successful measurement of the complex pressures at two closely spaced planes would permit acoustic particle velocities to be inferred, thus permitting calculation of the exit- or entrance-plane impedance. Although fraught with difficulty, this approach is being actively pursued by the development of inflow acoustic probes to directly measure acoustic pressure distributions in both the source and the exit planes. A second approach to acquiring source- and exit-plane pressure distributions is also being pursued. In this approach, acoustic pressure measurements are confined entirely to walls of the source and exit sections of the flow duct. These pressures are then used to construct the inflow pressure and particle velocity fields from a modal decomposition of the hardwall pressure measurements. The advantages of this approach are 1) the avoidance of inflow measurements and 2) the intuitive appeal and physical insight provided by the modal propagation model.

References

[1]Feder, E., and Dean L. W., III, "Analytical and Experimental Studies for Predicting Noise Attenuation in Acoustically Treated Ducts for Turbofan Engines," NASA CR-1373, 1969.

[2]Phillips, B., and Morgan, C. J., "Mechanical Absorption of Acoustic Oscillations in Simulated Rocket Combustion Chambers," NASA TN D-3792, 1967.

[3]Phillips, B., "Effects of High Value Wave Amplitude and Mean Flow on a Helmholtz Resonator," NASA TMX-1582, 1967.

[4]Armstrong, D. L., Beckemeyer, R. J., and Olsen, R. F., "Impedance Measurements of Acoustic Duct Liners with Grazing Flow," Boeing Paper, Acoustical Society of America 87th Annual Meeting, New York, April 1974.

[5]Watson, W. R., "A Method for Determining Acoustic-Liner Admittance in a Rectangular Duct with Grazing Flow from Experimental Data," NASA TP-2310, 1984.

[6]Watson, W. R., "A New Method for Determining Acoustic-Liner Admittance in Ducts with Sheared Flow in Two Cross-Sectional Directions," NASA TP-2518, 1985.

[7]Parrott, T. L., Watson, W. R., and Jones, M. G., "Experimental Validation of a Two-Dimensional Shear-Flow Model for Determining Acoustic Impedance," NASA TP-2679, 1987.

[8]Watson, W. R., Jones, M. G., Tanner, S. E., and Parrott, T. L., "A Finite Element Propagation Model for Extracting Normal Incidence Impedance in Nonprogressive Acoustic Wave Fields," NASA TM-110160, April 1995.

[9]Jones, M. G., and Parrott, T. L., "Evaluation of a Multi-Point Method for Determining Acoustic Impedance," *Mechanical System and Signal Processing Journal*, Vol. 3, No. 1, 1989, pp. 15–35.